Nanomanufacturing and Metrology (2025) 8:18
https://doi.org/10.1007/s41871-025-00265-w

ORIGINAL ARTICLE

Fabrication of Groove-with-Protrusion Surface Structures on Oxygen-Free Copper Using a Laser-Engineered Burnishing Tool

Asuka Otani[1] · **Jiwang Yan**[2]

Received: 17 January 2025 / Revised: 13 May 2025 / Accepted: 14 May 2025

Abstract

Microtextured surfaces, such as those with groove, hole, or protrusion structures, are widely used in various industries for bonding dissimilar materials because of their anchor effect, which enhances adhesion and penetration with other materials. Although surfaces with grooves and protrusions are expected to show higher bonding strength, it is difficult to fabricate such hybrid structures using a material removal process or additive manufacturing. This study established a new burnishing method using a tool with preformed microgrooves at the tip to fabricate groove-with-protrusion structures on metal surfaces by plastic deformation. The tip of a ball-shaped polycrystalline diamond (PCD) tool was irradiated with a femtosecond pulsed laser to generate multiple trapezoid ten-micron scale grooves. Burnishing was then conducted on an oxygen-free copper surface to investigate the characteristics and mechanism of the burnishing-induced plastic deformation behaviors. The results showed that protrusions and grooves, which were several tens of micrometers in height and depth, were simultaneously produced along the tool path on the material surface. Tool sliding on the workpiece induced shear stress, which mainly triggered dislocation movement and plastic deformation enhancement. Cross-sectional observation revealed that grain elongation and refinement remarkably increased with the burnishing depth, indicating that the shear stress from burnishing produced refined grains that flowed and formed the protrusions. This research demonstrates the feasibility of a highly efficient method for simultaneously generating groove-with-protrusion structures with enhanced surface properties.

Highlights

1. Protrusions and grooves were alternately and simultaneously formed on the workpiece due to the plastic flow of the material.
2. The compressive stress induced by the normal force and the shear stress induced by the tangential force promoted plastic flow, increasing the groove depth and protrusion height.
3. Crystal grains were elongated and refined by the motion of dislocations activated by shear stress on the groove surface and flowed to form a protrusion.

Keywords Burnishing · Structured surface · Surface texturing · Grain refinement · Laser-engineered tool

1 Introduction

Microtextured surfaces have been gaining much attention due to their ability to enhance surface functionality in various materials. Much research has reported the effects of microstructures, such as controllable wettability [1], improving corrosion resistance [2], and interfacial adhesiveness [3]. Numerous shape patterns, including grooves [1], grids [4], and protrusions [5], have been created depending on the required features. Therefore, surface structure is one of the crucial factors in determining the service performance

✉ Jiwang Yan
yan@mech.keio.ac.jp

[1] School of Integrated Design Engineering, Graduate School of Science and Technology, Keio University, Yokohama 223-8522, Japan

[2] Department of Mechanical Engineering, Faculty of Science and Technology, Keio University, Yokohama 223-8522, Japan

Published online: 24 July 2025

of components. Among these properties, the utilization of controllable adhesiveness to directly join dissimilar materials has received great interest. Direct bonding is one of the typical jointing techniques to incorporate polymers on metallic components through microstructures without using any adhesives or screws. Especially in the automotive and aeronautical industries, the combination of different materials is often adopted to reduce weight and the number of parts in structural components, such as electronic packages and automobile interiors.

The adhesion control by surface topography, namely, the anchoring effect, has been observed in various geometries. For example, cavity shapes, such as grooves, on metallic components act as pockets into which the polymer penetrates and solidifies [6, 7]. Also, the shapes sticking out from the material surface, e.g., protrusions on the metal side, can puncture the plastic side and provide greater strength against the forces applied to the bonding interface [5]. When only a groove shape is used, the shear stress is concentrated in the polymer, making joint strength highly dependent on the polymer's properties. By contrast, metal protrusions penetrating the polymer distribute the shear stress across both materials to mitigate fractures. Thus, hybrid structures with two different kinds of microstructures, i.e., groove-with-protrusion structures, are expected to show better bonding strength and offer significant advantages for applications where the polymer used has a low fracture toughness.

Although numerous methods exist for creating single kinds of structures, the literature on fabrication methods for hybrid structures is limited. Groove structures are conventionally created by material removal processes, such as cutting [8], laser processing [3], and etching [9]. Meanwhile, protrusions can be formed by additive manufacturing [10]. However, material removal can only create structures mainly in the area below the base metal, and additive manufacturing can only provide protrusions in the area above the base metal, it is difficult to create both structures in a single process. Although a protrusion shape can be formed by shaving the entire base material during removal processes, low machining efficiency remains a severe problem. Therefore, an alternative method is required to fabricate this hybrid structure easily and efficiently in a single process.

One promising approach is the burnishing process, a surface modification technique that compresses the material surface with a ball or roller tool to plastically deform the material [11, 12]. The applied pressure induces localized plastic deformation during the process. Owing to the larger diameter of the tool compared with the burnishing depth, the material undergoes deformation without removal. This phenomenon is generally called the plowing effect. The amount of strain applied to the material can be controlled by optimizing the burnishing depth, tool speed, and tool diameter, resulting in surface smoothing, improved wear resistance [13], residual compressive stress, and grain refinement on the topmost surface [14], which enhances the surface strength.

Previous studies applied this plastic deformation method for fabricating microtextured surfaces [15, 16]. They utilized the plastic flow of material on both sides of the tool trajectory and the formation of a pile-up. However, their tool was a ball shape, and only one groove could be formed per burnishing pass, resulting in poor processing efficiency. Thus, the use of a tool with a pregrooved tip would be a practical approach to fabricate multiple grooves and protrusions in one path of burnishing. Similar studies reported the efficient creation of microgroove surfaces in batches by cutting with a grooved tool [17]. When a tool with multiple microgrooves at the tip is used for burnishing, the material is expected to flow inside the tool grooves to form protrusions. Furthermore, plastic deformation causes grain refinement inside the workpiece, leading to the formation of a hybrid structure with high hardness. Since the tool is usually mounted and controlled on a lathe, localized machining and machining of 3-D surfaces can also be performed. Thus, this new method shows high potential for fabricating functional groove-with-protrusion structures with high efficiency. However, the related fundamental deformation behaviors and mechanisms are still unknown.

Owing to the considerable deformation resistance during burnishing, the tool material requires high hardness. Polycrystalline diamond (PCD) is a suitable burnishing tool material, which is made by sintering diamond particles with a binder, such as cobalt, under high temperature and pressure. It does not exhibit cleavage properties as opposed to monocrystalline diamond, thus preventing chippings and fractures when used in compressive plastic deformation. Various approaches are available for fabricating microstructures on PCD, but each method has its limitations and disadvantages. For instance, a focused ion beam [18] requires a long processing time, and electrical discharge machining causes diamond particle graphitization inside the material at temperatures above 700 °C due to the heat effect on the surface [19], potentially compromising the hardness of the PCD tool. By contrast, an ultrashort pulsed laser has been reported to suppress the thermal effect on the workpiece [20]. Thus, this study used a femtosecond pulsed laser to fabricate microgrooves on a PCD tool.

To investigate the characteristics and effectiveness of this new processing method, the plastic deformation behavior of the workpiece under forces applied in each axial direction must first be clarified. However, the analysis of such phenomenon in burnishing is complicated because the contact area between the tool and workpiece changes constantly, depending on the rise of the material in front of the tool, the elastic recovery of the material behind the tool, and the plastic flow in each direction.

Therefore, two experiments were carried out to separately analyze the forces exerted by the tool on the material in each direction and their effects on the plastic deformation. The first was an indentation experiment in which the tool was moved only in the *Z* direction to investigate the shape formed on the workpiece surface by normal force. The second was a burnishing experiment in which the tool was advanced in the *X* direction from the indentation state.

In this research, microgrooves were fabricated on the tip of a PCD tool by femtosecond pulsed laser irradiation. Indentation and burnishing experiments were then carried out using the laser-engineered tool. The effects of compression and shear deformation caused by the tool motion were evaluated by comparing the results of the two experiments. Differences in processed surface morphology and subsurface microstructural changes were also investigated. The tool surface was observed after indentation and burnishing experiments to examine its topographical changes, and the characteristics and mechanism of plastic deformation behavior during the process were identified. This study aims to provide a cost-effective fabrication method for groove-with-protrusion structures on metals.

2 Experimental Procedures

2.1 Fabrication of Laser-Engineered Tool

For laser-grooved tool fabrication, a femtosecond pulsed laser was irradiated onto the tip of a burnishing tool. The tool has a hemispherical shape at the tip, which is made of PCD, and the base material is tungsten carbide (Fig. 1a). As shown in Fig. 1b and the cross-sectional profile in Fig. 1c, the original surface area was smooth. In the close-up view of the tip in Fig. 1b, the area inside the white dashed line (500 µm diameter) is the region that contacts the workpiece during the experiment. Therefore, laser processing must be applied to the entire area within this circle.

Figure 2 shows the experimental setup of the femtosecond pulsed laser system (PHAROS-08–600-PP, manufactured by Light Conversion, Lithuania). The laser beam energy distribution is Gaussian, and the beam polarization is linear. As shown in Fig. 3a, the center of the PCD tool tip was aligned with the laser focus position. The laser was scanned by a galvanometer scanner in the *X* and *Y* directions so that grooves were machined at the position indicated by the white arrows. Each groove was fabricated at a scanning width of 40 µm

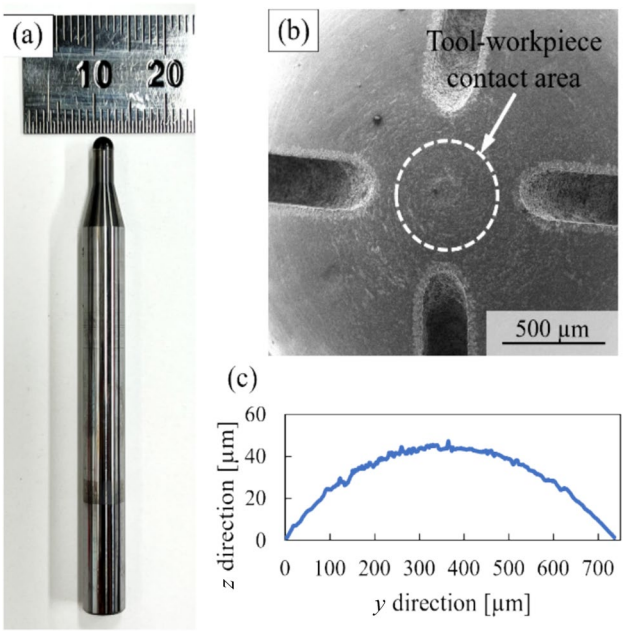

Fig. 1 Original PCD tool: **a** overall view; **b** SEM image; **c** surface profile

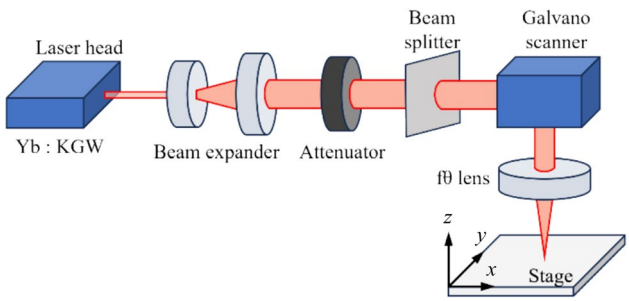

Fig. 2 Experimental setup for femtosecond pulsed laser irradiation

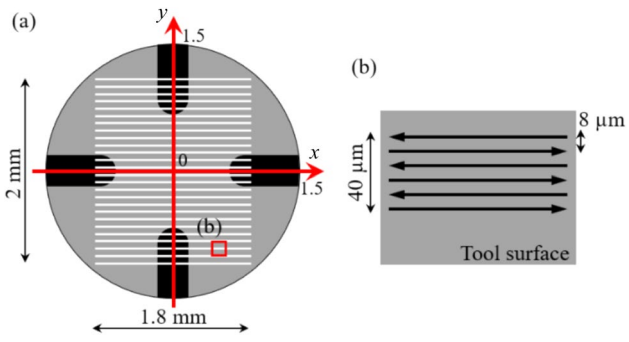

Fig. 3 Laser scanning path for fabricating grooves at the tip of the tool: **a** overall view of the scanning path on the tool tip; **b** enlarged view of the scanning path for a single groove

and a hatch width of 8 µm (Fig. 3b). The tool groove width was set to more than 40 µm, much larger than the workpiece's average grain size of 9.2 µm, to prevent plastic flow obstruction caused by collisions between grain boundaries and tool groove edges during burnishing. Laser scanning was conducted 40 times. The experimental conditions of laser irradiation are presented in Table 1.

After laser irradiation, the tool surface was observed using a field emission scanning electron microscope (FE-SEM). Figures 4a and b show the overall images of the PCD tool tip after laser irradiation. Every groove had microtextures at the bottom and the nanometer-scale stripe patterns on its side parts due to the influence of laser processing (Fig. 4c). Figure 4d displays the high-magnification image of one groove with formed edges. Microscopic irregularities were observed on the bottom surface of every groove. During burnishing, these rough structures will capture materials when the bottom of the groove surface comes in contact with the workpiece. To mitigate the severe adhesion of materials due to frictional contact with the workpiece during burnishing, this study set the burnishing depths to be smaller than the tool groove depth.

Twenty-six trapezoidal grooves were fabricated, of which four positioned at $y = -120, -40, 40, 120$ µm were in the contact region. Figure 5 indicates the variation of depth and width of each groove along the X direction. As shown in Fig. 5a, the groove depth remained constant along the X direction for all grooves. By contrast, Fig. 5b indicates that the groove width was greater near the center of the tool but narrowed by approximately 8 µm at the edges of the contact region. This variation is presumably due to a height difference of approximately 14 µm between the center and edge regions. The laser focus point was adjusted at the center of the tool surface, causing a difference in groove width. This PCD tool was used throughout the experiments.

2.2 Burnishing and Indentation Experiments

Oxygen-free copper was chosen as the workpiece material for burnishing and indentation experiments. The workpiece dimensions are 15 × 15 × 3 mm. The workpiece used in the indentation experiment was prepolished. For the burnishing experiments, which involves tool movement in the X direction, surface flattening by an ultraprecision cutting machine was performed on the workpiece beforehand to reduce processing errors from surface inclination. The Young's

Table 1 Laser irradiation conditions

Laser medium	Yb:KGW
Wavelength [µm]	1028
Pulse width [fs]	256
Spot diameter [µm]	16
Repetition rate [kHz]	100
Laser fluence [J/cm^2]	2.0
Scanning speed [mm/s]	60
Number of irradiations	40

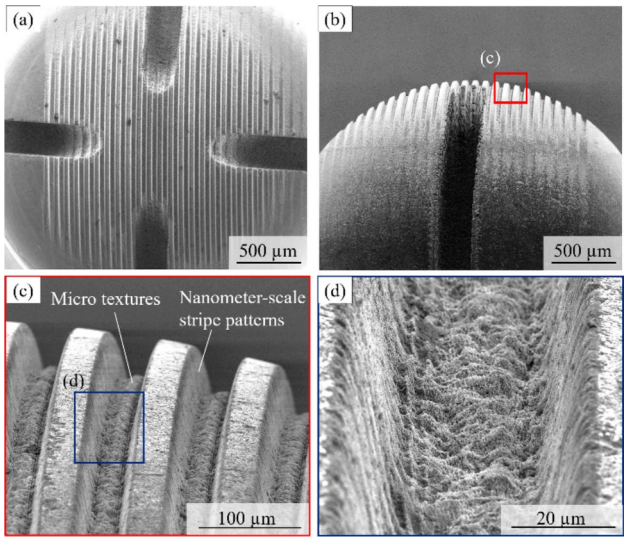

Fig. 4 SEM images of the tool surface after laser irradiation: **a** top view; **b** side view; **c** enlarged view of grooves; **d** enlarged view of the inside of a single groove

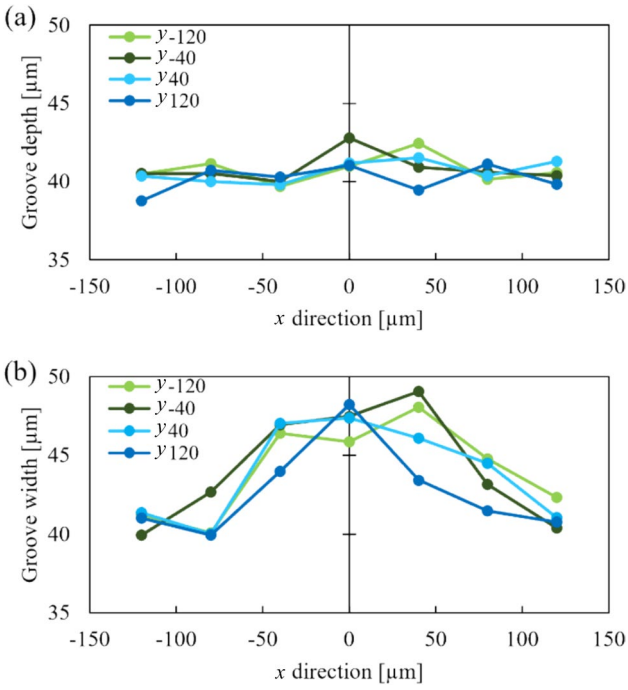

Fig. 5 Variation in **a** depth and **b** width of grooves formed around $y = -120, -40, 40$ and 120 µm

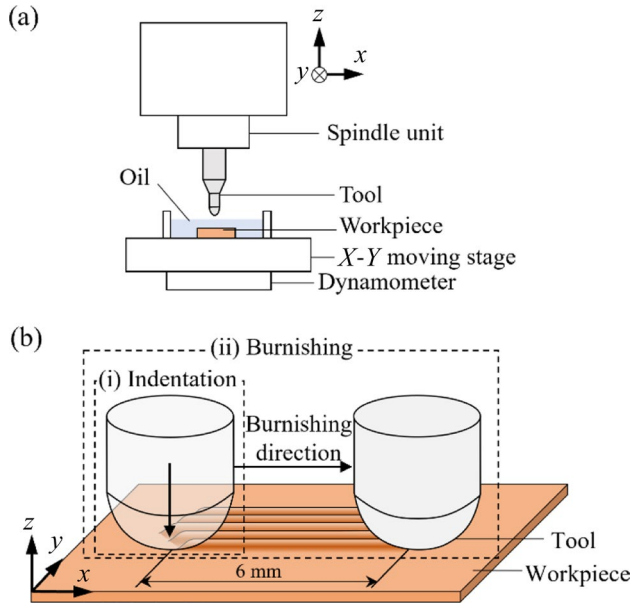

Fig. 6 Schematics of **a** burnishing system and **b** indentation and burnishing experiments

Table 2 Experimental parameters used in the burnishing and indentation tests

	Indentation	Burnishing
Burnishing/indentation depth [μm]	9, 15, 23	9, 15, 23
Speed (*Z*-direction) [mm/s]	0.05	0.05
Speed (*X*-direction) [mm/s]	–	2.0
Environment	Dry	With oil

modulus, yield stress, and tensile strength are 117 GPa, 200 MPa, and 230 MPa, respectively.

Figure 6a shows a diagram of the burnishing system. The tool was attached perpendicular to the workpiece, which was fixed on the stage using wax, and the tool groove was adjusted to be parallel to the *X* direction. Figure 6b demonstrates the diagram of the two experiments: first is when the tool was moved only in the *Z* direction as indentation, and second is when it was slid 6 mm in the *X* direction for burnishing. The burnishing/indentation depths were 9, 15, and 23 μm. Oil was used for lubrication to avoid material adhesion to the tool surface. The detailed parameters for each experiment are summarized in Table 2. Forces applied by tool movement were monitored using a piezoelectric dynamometer (9256 C2, Kistler Co., Ltd., Switzerland) throughout the experiments. After both experiments, the burnished groove-with-protrusion structures were observed using FE-SEM. The cross-sectional profiles were measured by scanning white light interferometry, and microstructural changes in subsurface layers were characterized by electron backscatter diffraction pattern analysis. Furthermore, the tool surface condition after burnishing was verified by SEM and energy dispersive X-ray spectroscopy.

3 Results and Discussion

3.1 Surface Morphology of the Workpiece After Burnishing

Figure 7 shows the overall workpiece surface and magnified images of the workpiece when burnishing was performed at three different burnishing depths. Protrusions and grooves were formed alternately and continuously along the *X* direction and uniformly generated in line with the groove gap on the tool. No chips were observed during burnishing, indicating that these surface microstructures were formed through plastic deformation. In the enlarged views in Fig. 7d, e, and f, the bottom surface of the grooves exhibited streaks parallel to the tool movement direction, suggesting the occurrence of sliding contacts between the tool groove surface and workpiece. This surface morphology is similar to that achieved with conventional ball or roller burnishing.

By contrast, pile-ups containing shear zones were randomly observed on both sides of the protrusion surface. Given that the preflattened surface remained at the center of the protrusion, the inference is that no contact occurred between the surface and the bottom of the tool, indicating that these structures were formed solely through plastic flow.

Based on the above results, it can be deduced that the grooved tool initially glides over the workpiece during burnishing, effectively smoothing the central region of the grooves. The workpiece material then flowed into the tool groove by plastic flow and was deposited, leading to pile-ups at both ends of the protrusion. It is worth noting that irregularities on the protrusion surface displayed significant nonuniformity. One possible reason for this phenomenon is the effect of the crystallographic orientation of polycrystalline copper. The randomly oriented crystal grains inside the workpiece caused different slip plane directions, which resulted in variations in the direction of slip deformation under applied forces [21]. This lack of uniformity influenced the plastic flow's height and orientation, leading to irregularities on the top surface of protrusions. Another reason could be the slight misalignment between the tool groove direction and the *X*-direction of the stage. If the tool groove orientation is precisely controlled in the experimental setup, the unevenness of the protrusions can be minimized, allowing for the fabrication of uniform structures. This misalignment of tool direction will result in changes to plastic flow and deviations of groove depth and protrusion height within

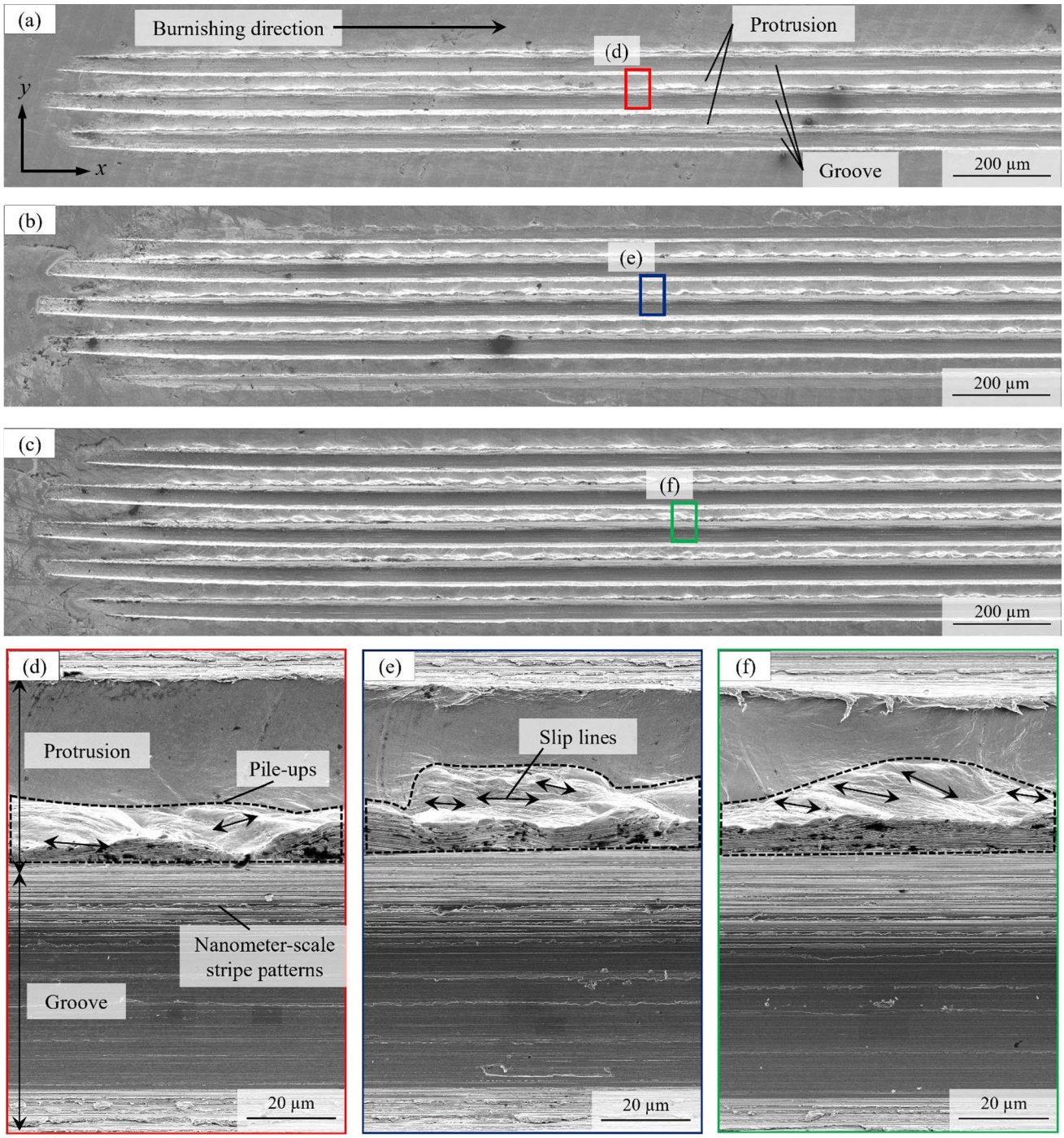

Fig. 7 SEM images of the burnished surfaces under a burnishing depth of **a** 9 µm, **b** 15 µm, **c** 23 µm; **d–f** corresponding close-up views of the surface regions for each burnishing depth

several micrometers. Nevertheless, these changes have a minimal impact on structural functionality because the overall structure size is several tens of micrometers.

3.2 Comparison of Burnishing and Indentation Results

The surface morphology and cross-sectional profiles of the workpiece were compared after burnishing and indentation experiments to investigate the effect of tool movement

changes on the plastic flow of the material. Figure 8a and d show the overall and enlarged views of the workpiece for each experiment under a burnishing/indentation depth of 15 µm. Although protrusions and grooves were formed continuously in both experiments, the bottom parts of the grooves and the topmost surfaces of the protrusions differed significantly. As shown in Fig. 8b and e, the material surface exhibited the same morphology as the tool surface during indentation, while the groove surface in burnishing consisted of a smoothed central part and side parts with machining marks generated by friction against the lateral area of the tool groove. Moreover, Fig. 8c illustrates that the prepolished surface remained on the protrusion area after indentation, and no pile-ups occurred, unlike in Fig. 8f. Figure 9 displays the cross-sectional profiles of the workpiece surface. The groove depth increased by 43% to 51% in burnishing compared with that in indentation. Additionally, while the protrusion in the indentation remained flat with a height of approximately 4 µm, in burnishing, one side of the protrusion rose to a maximum height of 18.2 µm, and the protrusion width decreased.

In the indentation experiments, only normal force was applied from the tool to the material, causing the expansion

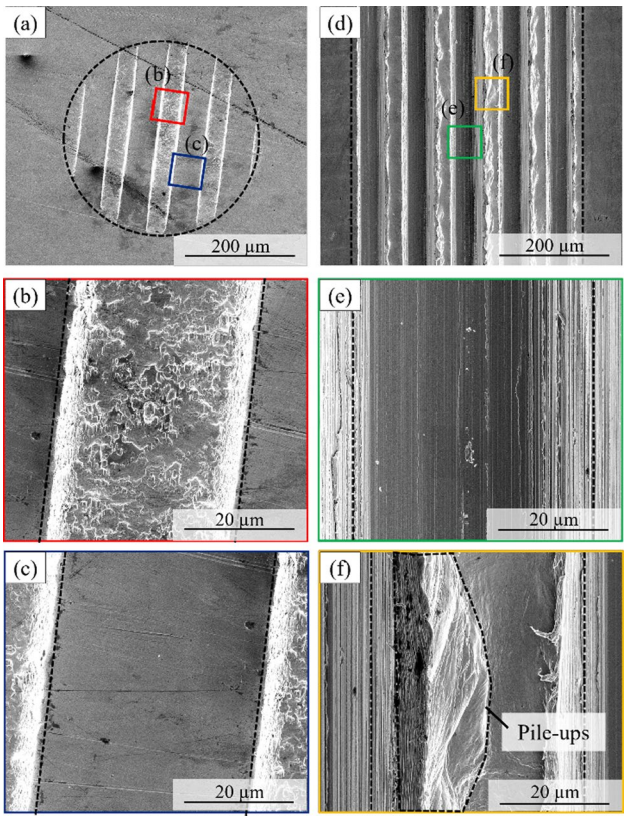

Fig. 8 SEM images of surfaces: **a** indentation, depth 15 µm; **b** and **c** are close-up views of the regions indicated in (**a**); **d** burnishing, depth 15 µm; **e** and **f** are close-up views of the regions indicated in (**d**)

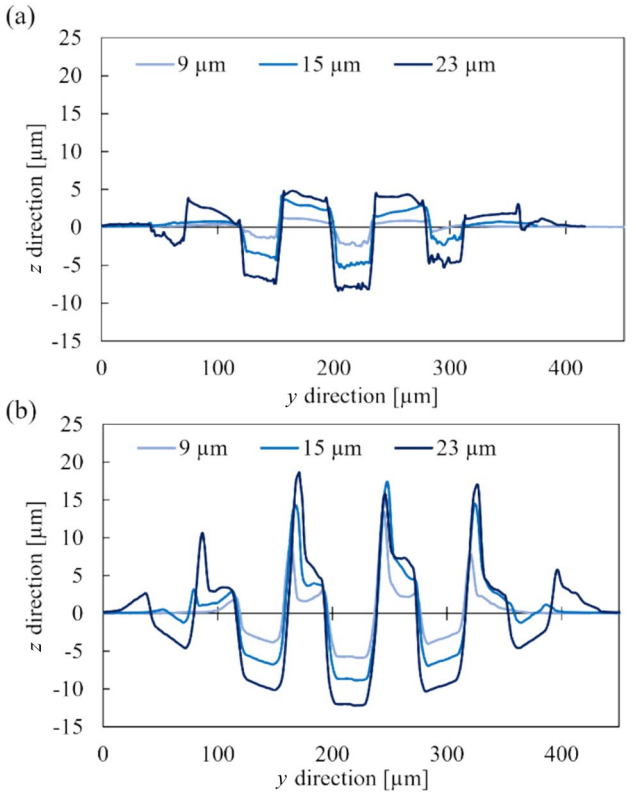

Fig. 9 Cross-sectional profiles of surfaces after **a** indentation and **b** burnishing

of compressive stress inside the workpiece in three dimensions and leading to flow in the *XY*-plane direction. Meanwhile, frictional forces were generated as the tool moved in the *X* direction during burnishing, thus applying shear stress inside the material and accelerating the plastic flow.

A previous study reported that polymer–metal bonding was successful when the microstructure aspect ratio exceeded 0.1, but structures with aspect ratios below 0.1 rarely bonded [20]. In the present work, the fabricated microstructures exhibited aspect ratios ranging from 0.2 to 0.4 across all burnishing depths, which is expected to be sufficient for polymer–metal direct bonding. Although the aspect ratio differed between the center and edges of the burnished area, uniform groove-with-protrusion structures can still be achieved by adjusting the tool path with the groove pitch and overlapping passes during large-area processing. In addition, most microstructures used in direct bonding are 1–100 µm in size, with deviations of only a few microns reported in many studies. Therefore, the proposed method meets this processing accuracy requirement.

The proportion of the workpiece material that was compressed inward and the proportion that flowed upward were calculated to analyze the amount of material flow. With *A* as the cross-sectional area that protrudes above the original surface of the workpiece and *B* as the cross-sectional area

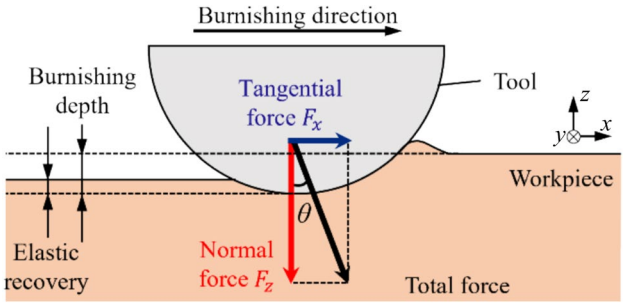

Fig. 10 Schematic of the forces in each direction that occurred during burnishing experiments

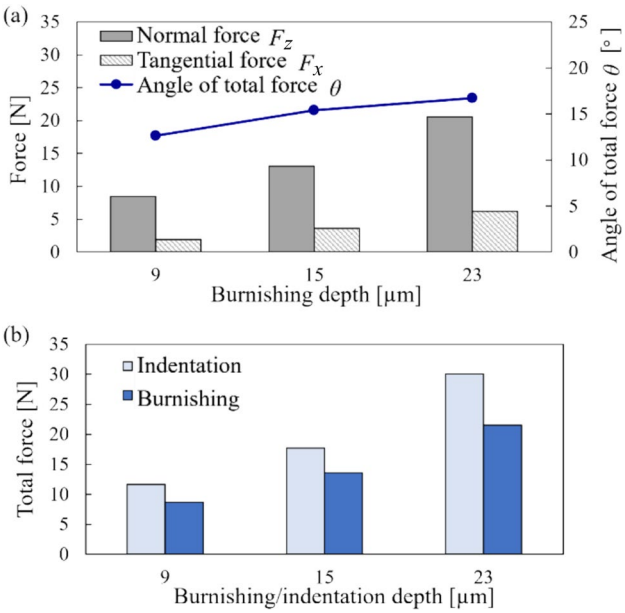

Fig. 11 **a** The amount of normal and tangential force during the burnishing experiments; **b** comparison of total forces of indentation and burnishing experiments

that is void at the bottom, *A/B* represents the proportion of the workpiece that is raised from below to above through plastic flow. The calculation results were 99.6%, 99.1%, and 73.2% under burnishing depths of 9, 15, and 23 μm, respectively. The results indicate that at 9 and 15 μm burnishing depths, almost all the workpiece material flowed. Meanwhile, around 27% of the copper was compressed into the groove rather than flowing into the protrusion at a burnishing depth of 23 μm.

The forces applied by the tool movement were analyzed to further investigate the relationship between tool movement and plastic deformation for each burnishing depth. Figure 10 is a schematic of the forces occurring in each direction during the experiments. The normal force (F_x), tangential force (F_z), and angle of total force (θ) are indicated in Fig. 11a. With an increase in burnishing depth, both forces progressively grew and θ incrementally rose. This finding indicates that the total force showed a gradual upward inclination toward the front of the tool. This inclination of total force generated increasingly high protrusions as the burnishing depth increased from 9 μm to 15 μm. In addition, large burnishing depths led to an expansion of the contact area between the tool and the material. Under a burnishing depth of 23 μm, the cross-sectional profile revealed the predominance of compression under the material surface despite the increased shear force. This phenomenon may be attributed to the enlarged contact area, which facilitates the entrapment of a large amount of material beneath the tool surface. As a consequence, the plastically deformed material is significantly distorted under elevated pressure, and the upward material flow is lessened.

Figure 11b shows the comparison of total forces between indentation and burnishing. Total force refers to the resultant force of F_x and F_z in burnishing and the normal force in indentation. In all the experiments, the total force in burnishing was consistently smaller than that in indentation. In accordance with Newton's third law, this finding indicates a reduction in the deformation resistance subjected to the tool by the workpiece. The sliding motion of the tool in the *X* direction caused a decrease in contact area compared with that during indentation. As a consequence, the applied pressure increased, and the induced shear strain facilitated the flow of the material from the front to the lateral sides of the tool groove. This phenomenon may contribute to the formation of larger grooves and protrusions. Therefore, groove-with-protrusion structures can be formed by two types of material deformation: the workpiece material is extruded by compression in the normal direction and flows laterally from the front of the tool due to shear stress. Based on the above results, the plastic flow behavior of the workpiece is significantly influenced by shear stress in burnishing, which makes this approach practical for fabricating groove-with-protrusion structures with smaller tool stress.

3.3 Subsurface Microstructural Changes After Burnishing

Cross-sectional observations and local strain distribution measurements were conducted to further investigate the plastic flow in the subsurface layer of the workpiece. Figure 12 shows the IPF and KAM maps of the groove cross-sections at different burnishing depths. In Fig. 12a1 and a2, the colloidal silica from polishing (sample preparation) remained at the edges of the groove, preventing the observation of the groove sidewalls, and only the groove bottom was visible. The blue dashed line indicates the top surface of the workpiece. The linear striations in each image were generated during the cross-sectional preparation of the workpiece

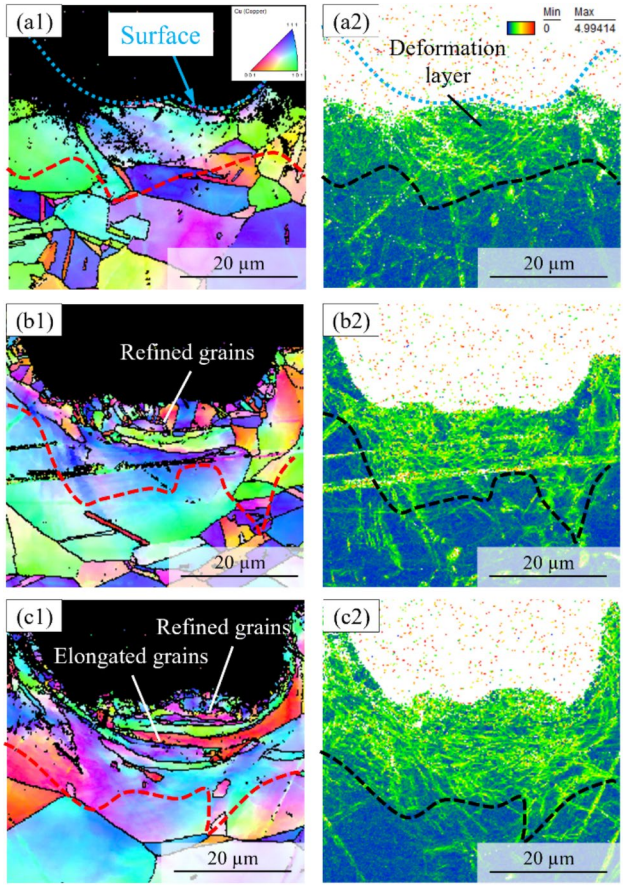

Fig. 12 IPF and KAM mappings of the bottom of burnished groove surfaces under a burnishing depth of **a** 9 µm, **b** 15 µm, and **c** 23 µm

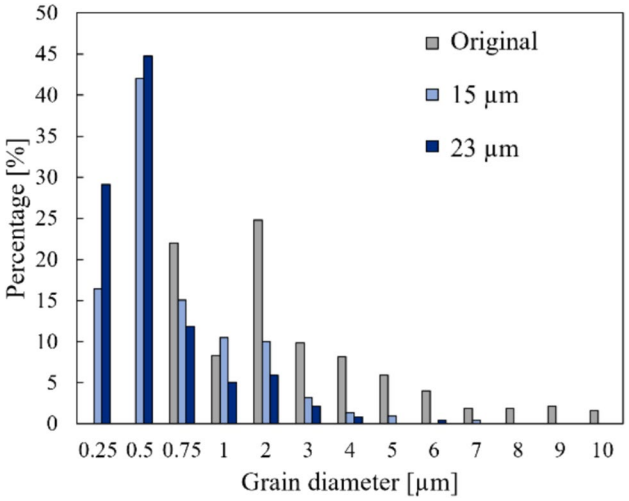

Fig. 13 Comparison of grain size distribution at the topmost surface of the grooves

through polishing. The residual effects of polishing were evident in oxygen-free copper, which is a ductile material. Given that these striations were uniformly distributed across the observed regions, their influence on the comparative analyses of different sections is considered negligible.

Figures 12a1, b1, and c1 indicate that the grain refinement near the top surface became significant with the increasing burnishing depth. The average grain size on the surface decreased from 9.2 µm (before the experiment) to 1.3 µm under a burnishing depth of 23 µm. As shown in Fig. 12c1, some elongated grains were observed beneath the refined grains, perpendicular to the tool motion. Figures 12a2, b2, and c2 also reveal that the dislocations inside the deformation layer increased in density and depth with the increasing burnishing depth. This finding indicates that the dislocations were composited by the shear stress generated by the tangential forces. Given that the workpiece was a polycrystalline, these dislocations accumulated near the grain boundaries. Therefore, the grains in the subsurface layers were likely elongated by tool loading and then divided into fine grains. Since sub-crystalline grain boundaries are formed when the dislocation density reaches a certain degree, grain elongation and refinement presumably occurred due to dislocation movement [14].

Figure 13 indicates the grain size distribution at the topmost surface of the original workpiece and the workpiece after the experiments under burnishing depths of 15 and 23 µm. The results demonstrated that the grain size tended to be decreased as the burnishing depth increased. Plastic deformation was less likely to occur on the topmost surface when the grain boundary increased due to this refinement. Therefore, since materials containing fine grains have high strength, the groove-with-protrusion structures formed by burnishing are high-strength surfaces composed of refined grains. This grain refinement is particularly important in direct bonding, where microstructures on the metal are subjected to shear stress. Since it is challenging to achieve these microstructural changes through microfabrication using other material removal processes or additive manufacturing, burnishing offers an advantage for fabricating microstructures with high strength.

The internal structural changes in protrusions and grooves were compared. Figure 14 shows the IPF and KAM maps of the protrusion at a burnishing depth of 15 µm. Figures 14b1 and c1 reveal that on the groove surface, the deformation layer reached a size of approximately 20 µm from the top surface. Meanwhile, it was only 4–5 µm on the protrusion surface. Grain shape analysis showed that fine grains were observed near the top of the protrusion, even though the protrusion was not in contact with the tool surface. The inner part of the pile-up observed at both ends of the protrusion was composed of fine grains, the amount of which decreased toward the center. This result indicates that some of the elongated and refined grains, formed due to compression and shear stress by the tool movement, flowed inside the tool

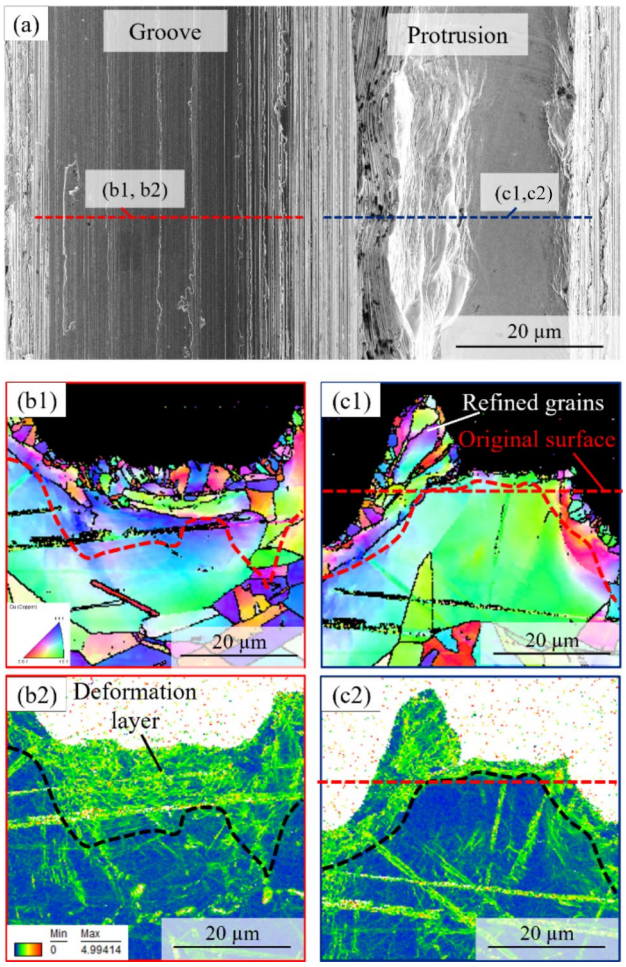

Fig. 14 **a** SEM image of groove and protrusion at the burnished surface under a burnishing depth of 15 μm; **b** and **c** are cross-sectional IPF and KAM mappings along the red and blue dashed lines indicated in (**a**), respectively

groove and formed protrusions. A comparison of dislocation densities in Fig. 14b2 and c2 also indicates that the protrusion formation was due to the dislocation movement inside the subsurface layer of the workpiece. These observations reveal the basic formation mechanism of grooves and protrusions during burnishing with a grooved tool.

3.4 Tool Surface Topographical Changes

The surface condition of the tool after burnishing was investigated. In general, the contact area between the tool and workpiece during burnishing is larger than that during other machining processes, causing friction and the adhesion of the workpiece material to the tool surface. Figure 15 shows the SEM images of the tool surface, and Fig. 16 shows the elemental mapping image of the top surface of the groove. Copper adhered to the irregularities of the top surface of the groove. These irregularities existed before laser irradiation,

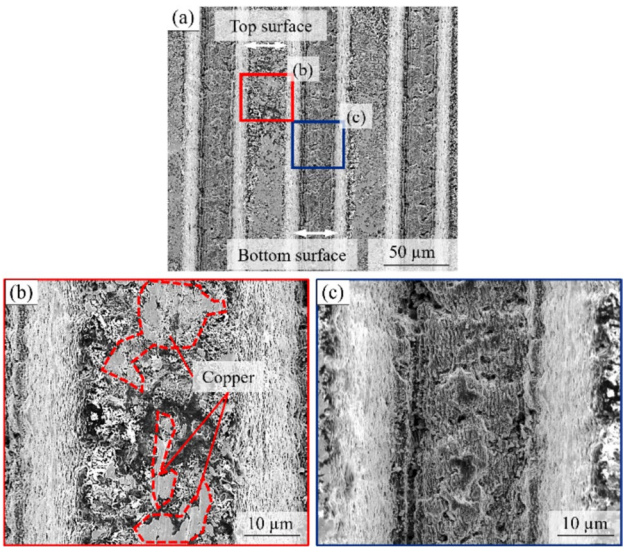

Fig. 15 SEM images of the tool surface after burnishing: **a** overall view; **b** enlarged view of the top surface of groove; **c** enlarged view of the bottom surface of the groove

caused by the PCD structures made by diamond particles hardened with cobalt as a binder. If a tool with small surface roughness is utilized, then the amount of adhesion will be reduced. In addition, copper adhesion was rarely observed inside the tool groove and the entire contact area. The reason is that the depth of the tool groove was sufficiently large compared to the burnishing depth, and a gap existed between the tool surface and the workpiece surface, which played the role of an oil pocket. This area served as a lubricant oil film between the workpiece and the tool surface, helping to prevent excessive adhesion [22]. Since little material adhesion was observed on the tool surface after all the experiments,

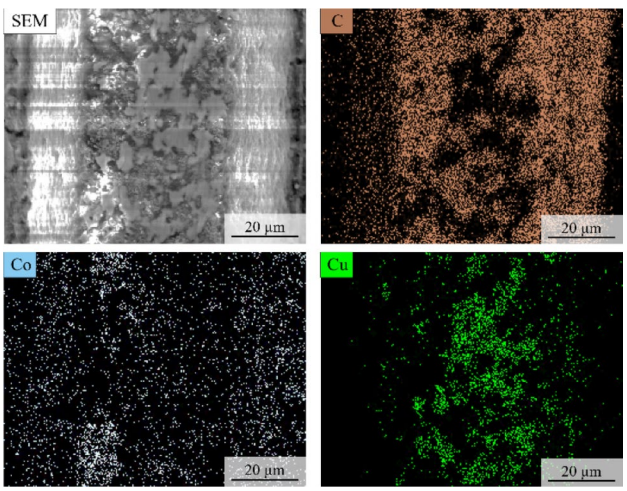

Fig. 16 Elemental mappings of the top surface of the tool groove after burnishing

the tool can be used repeatedly to continuously fabricate groove-with-protrusion structures. The optimal processing parameter must be within a range that can achieve sufficient grain refinement on the workpiece surface without inducing material adhesion on the tool surface. In this study, a burnishing depth of 23 μm was selected as the optimal parameter.

4 Conclusions

A ball-shaped PCD tool was irradiated by a femtosecond pulsed laser to generate grooves on the tool tip. Indentation and burnishing experiments were then conducted using this tool to fabricate groove-with-protrusion structures. The characteristics and mechanisms of plastic deformation during this process were investigated. The following conclusions were obtained:

- Protrusions and grooves were simultaneously formed on the workpiece due to the plastic deformation of the material in both experiments.
- The compressive stress induced by the normal force and the shear stress caused by the tangential force promoted plastic flow, thereby increasing the groove depth and protrusion height. Shear stress significantly promoted the plastic flow behavior of the workpiece during burnishing.
- The burnished surface consisted of crystal grains that were elongated and refined by the dislocation motion, which was activated by the shear stress on the groove surface and flowed to form a protrusion.
- Minimal material adhesion was observed on the tool surface after burnishing and was attributed to the lubrication oil film between the workpiece and the tool surface.

These findings clarify the characteristics of burnishing with a laser-engineered tool and the mechanism of plastic deformation. This work shows the possibility of extending its applications to the fabrication of functional surfaces, especially for metal–polymer bonding in industrial fields.

Author Contributions Asuka Otani: Conceptualization, Formal analysis, Investigation, Data curation, Original draft; Jiwang Yan: Conceptualization, Methodology, Supervision, Funding acquisition, Review & Editing.

Data Availability No data is associated with the manuscript.

Declarations

Competing interests Jiwang Yan is an editorial board member for "Nanomanufacturing and Metrology" and was not involved in the editorial review, or the decision to publish this article. The authors declare that they have no known competing financial interests or personal relationships that could have appeared to influence the work reported in this paper.

References

1. Song D, Song B, Hu H, et al (2015) Contact angle and impinging process of droplets on partially grooved hydrophobic surfaces. Appl Thermal Eng 85:356–364. https://doi.org/10.1016/j.applthermaleng.2015.03.071
2. Rafieazad M, Jaffer JA, Cui C, et al (2018) Nanosecond laser fabrication of hydrophobic stainless steel surfaces: the impact on microstructure and corrosion resistance. Materials 11(9):1577. https://doi.org/10.3390/ma11091577
3. Nakajima A, Omiya M, Yan J (2022) Generation of micro/nano hybrid surface structures on copper by femtosecond pulsed laser irradiation. Nanomanufac Metrol. 5:274–282. https://doi.org/10.1007/s41871-022-00135-9
4. Li H, Wang X, Zhang J, et al (2022) Experimental investigation of laser surface texturing and related biocompatibility of pure titanium. Int J Adv Manufac Technol 119:5993–6005. https://doi.org/10.1007/s00170-022-08710-6
5. Iwata K, Suzuki A, Kim SG, et al (2022) Enhancing the solid-state joinability of A5052 and CFRTP via an additively manufactured micro-structure. J Mater Process Technol 306:117629. https://doi.org/10.1016/j.jmatprotec.2022.117629
6. Taki K, Nakamura S, Takayama T, et al (2016) Direct joining of a laser-ablated metal surface and polymers by precise injection molding. Microsyst Technol 22:31–38. https://doi.org/10.1007/s00542-015-2640-2
7. Kajihara Y, Tamura Y, Kimura F, et al, Yamaguchi E (2018) Joining strength dependence on molding conditions and surface textures in blast-assisted metal-polymer direct joining. CIRP Ann 67:591–594. https://doi.org/10.1016/j.cirp.2018.04.112
8. Kurniawan R, Kumaran ST, Ali S, et al (2018) Experimental and analytical study of ultrasonic elliptical vibration cutting on AISI 1045 for sustainable machining of round-shaped microgroove pattern. Int J Adv Manufac Technol 98:2031–2055. https://doi.org/10.1007/s00170-018-2359-1
9. Han G, Sasaki M (2022) Microtextured die using silicon stencil mask for micro-machining of stainless steel. Jpn J Appl Phys 61: SA1012. https://doi.org/10.35848/1347-4065/ac1c3b
10. Webster S, Lin H, Carter FM, et al (2021) Physical mechanisms in hybrid additive manufacturing: a process design framework. J Mater Process Technol 291:117048. https://doi.org/10.1016/j.jmatprotec.2021.117048
11. Zhang Q, Ye Y, Yang Y, et al (2022) A review of low-plasticity burnishing and its applications. Adv Eng Mater 24(11): 2200365. https://doi.org/10.1002/adem.202200365
12. Priyadarsini C, Venkata Ramana VSN, Aruna Prabha K, et al (2019) A review on ball, roller, low plasticity burnishing process. Mater Today Proc 18:5087

13. Yilmaz H, Sadeler R (2019) Impact wear behavior of ball burnished 316L stainless steel. Surface Coatings Technology. 363:369–378. https://doi.org/10.1016/j.surfcoat.2019.02.022
14. Zhang X, Luo H, Han Z, et al (2014) Evolution of microstructures and texture in the surface layer of copper during burnishing process. Mater Sci Technol (United Kingdom) 30:1742–1750. https://doi.org/10.1179/1743284713Y.0000000463
15. Zhang B, Wang Q, Shen N, et al (2017) Experimental investigation and numerical analysis of mechanical ruling for an aluminum-coated diffraction grating. J Manufac Sci Eng, Trans ASME 139(2):021003. https://doi.org/10.1115/1.4034282
16. Hou X, Mankoci S, Walters N, et al (2018) Hierarchical structures on nickel-titanium fabricated by ultrasonic nanocrystal surface modification. Mater Sci Eng C 93:12–20. https://doi.org/10.1016/j.msec.2018.07.032
17. Takayama N, Ishizuka J, Yan J (2018) Microgrooving of a single-crystal diamond tool using a picosecond pulsed laser and some cutting tests. Precision Eng 53:252–262. https://doi.org/10.1016/j.precisioneng.2018.04.009
18. Maeng S, Ito H, Kakinuma Y, et al (2023) Study on cutting force and tool wear in machining of die materials with textured PCD tools under ultrasonic elliptical vibration. Int J Precision Eng Manufac - Green Technol, Korean Soc Precision Eng 10:35–44. https://doi.org/10.1007/s40684-022-00416-0
19. Pratap A, Patra K, Dyakonov AA (2019) On-machine texturing of PCD micro-tools for dry micro-slot grinding of BK7 glass. Precision Eng 55:491–502. https://doi.org/10.1016/j.precisioneng.2018.11.004
20. Trucchi DM, Bellucci A, Girolami M, et al (2017) Surface texturing of CVD diamond assisted by ultrashort laser pulses. Coatings 7(11): 185. https://doi.org/10.3390/coatings7110185
21. Gao Z, Peng L, Yi P, et al (2015) Grain and geometry size effects on plastic deformation in roll-to-plate micro/meso-imprinting process. J Mater Process Technol, 219:28–41. https://doi.org/10.1016/j.jmatprotec.2014.12.005
22. Tang Y, Chi Y, Chen JC, et al (2007) Experimental study of oil-filled high-speed spin forming micro-groove fin-inside tubes. Int J Mach Tools Manuf 47:1059–1068. https://doi.org/10.1016/j.ijmachtools.2006.10.001

Asuka Otani received her bachelor's degree in mechanical engineering from Keio University in 2023. She is currently a master's degree graduate student in integrated design engineering at Keio University under supervision of Prof. Jiwang Yan. Her research interests are ultraprecision machining.

Jiwang Yan received his Ph.D. from Tohoku University, Japan in 2000 and is currently a professor of Mechanical Engineering at Keio University (2012-now), leading the Laboratory for Precision Machining and Nano Processing. His research areas include ultraprecision machining, micro/nano manufacturing, laser processing, nanomaterials, and nanomechanics.